Nonlinear Dyn (2020) 102:907–925
https://doi.org/10.1007/s11071-019-05441-4

ORIGINAL PAPER

Synchronization and chimera state in a mechanical system

Phablo R. Carvalho · Marcelo A. Savi

Received: 7 September 2019 / Accepted: 16 December 2019 / Published online: 3 January 2020
© Springer Nature B.V. 2020

Abstract Synchronization phenomenon appears in several natural systems being associated with physical, chemical and biological processes. In brief, synchronization may be understood as a harmonization of two or more system behaviors following some patterns. This paper deals with synchronization analysis of a mechanical pendulum-chart system composed by a hierarchical network of three pendula coupled to each other through their own chart that receives continuous supply of energy via a base excitation. Dynamical patterns are classified and investigated in order to understand the conditions to each one of them. Asynchronous behaviors are analyzed including the chimera state defined as a symmetry break of the behavior of identical oscillator network. Numerical simulations indicate that patterns do not have a direct relation with periodicity. An energetic approach is proposed in order to define a measure of synchronized states, providing new insights about the origin of chimera state and its relationship with natural frequencies.

P. R. Carvalho · M. A. Savi (✉)
Center for Nonlinear Mechanics, COPPE – Department of Mechanical Engineering, Universidade Federal do Rio de Janeiro, 21.941.972, P.O. Box 68.503, Rio de Janeiro, RJ, Brazil
e-mail: savi@mecanica.ufrj.br

P. R. Carvalho
e-mail: pr.carvalho@mecanica.coppe.ufrj.br

Keywords Nonlinear dynamics · Chaos · Synchronization · Chimera states · Mechanical system · Mechanical oscillators

1 Introduction

Rhythms are an essential characteristic of natural systems being associated with several patterns. Synchronization is one of these phenomena, being defined as a combination of two or more system behaviors following some pattern. Huygens [1] was the first scientist that discussed the synchronization phenomenon in 1665 investigating clocks based on pendulum oscillations. Although the analysis was essentially the pendulum synchronization, the phenomenon was called "sympathy" between the clocks [2]. Basically, the analysis was developed considering a system of two pendulum clocks hanging on the same base and the idea was to exploit the clock oscillation on the same frequency, either in-phase or anti-phase. Results of Huygens [1] was recreated by Kapitaniak et al. [3] and Bennet et al. [4].

Nature presents several examples of synchronous behavior as the synchronization of fireflies on the southeast of Asia [5], applauses [6] or chirps of crickets [7]. Thereby, the synchronization is a collective behavior of animals and physical system as the Huygens' clocks [1].

The first mathematical investigation of synchronization was provided by Wiener [8,9] that developed a

model for the neural system based on Fourier integrals, obtaining a frequency distribution similar to brain α-rhythm. Winfree [10] reformulated the problem in terms of a large population of coupled limit-cycle oscillators allowing the observation of the long period of synchrony. The quantification of synchronization is a challenging topic, and it is usual to employ the order parameter, first proposed by Kuramoto [11].

Several experiments are being developed in order to investigate synchronization phenomenon. Coupled metronomes are often employed due to the self-sustained behavior [3,12–17]. Synchronization of rotational pendula [18], four non-rotational pendula on the same base with an harmonic excitation on the ensemble [19], three pendula with a horizontal base excitation [20,21] are some examples.

The Millennium bridge, opened at 2000 in London, becomes one of the most important symbols of the synchronization as a spontaneous phenomenon. In brief, the bridge presents a sideway oscillation due to the people walk. The interaction between pedestrians and the bridge structure produces a synchronization where pedestrians feel a vibration on their feet, being induced to walk on the same frequency of the bridge, amplifying the bridge vibration [22].

Network synchronization is another interesting topic related to the general synchronization phenomenon. The model of phase oscillators was employed in different situations to describe complex network synchronization [23–26]. Hierarchical network is a typical situation related to synchronization with directional coupling and master–slave configuration. Semiconductor lasers are examples of application of this network configuration to increase the intensity of the beam [27]. Synchronization of chaotic systems is another possibility treated in the literature [28–35].

Power grid networks also exploit synchronization aspects trying to reach a situation as much decentralized as possible, being less susceptible to external perturbations. Synchronization in decentralized networks makes the operation more stable [36–40]. This idea can be applied to communication networks where each computer integrated to the network has its own frequency and interacts to others exchanging information. The use of synchronization in these networks makes easier the information exchange and reduces the energy consumption [41–46]. Comparing the cost of a master–slave network to a fully connected, the second is cheaper and reliable, remaining the system synchronized even if one component fails [47]. The control of coupled oscillators model is treated in some references [48–50].

Kuramoto and Battogtokh [51] found interesting results in a ring of identical oscillators, concluding that some oscillators achieve a synchrony steady state while others remain desynchronized. This break of symmetry was later named by Abrams et al. [52] as chimera state that is formally defined as a break of symmetry in identical oscillators with symmetric couplings. This behavior was initially counterintuitive since partial synchronization was only observed in systems with asymmetric topology or with distinct oscillators [53]. Thereby, the chimera state is a complex dynamical pattern on systems with symmetric oscillators and regular topology.

After these pioneer works, chimera state was observed in different situations but always in a theoretical way [54]. Only in 2012 two experimental setups achieved the chimera state in photosensitive chemical reactions [55,56]. Afterward, a mechanical experimental apparatus composed by coupled metronomes reached the chimera state [57]. Kapitaniak et al. [58] observed the same behavior in a ring of coupled metronomes and Wojewoda et al. [59] reduced the system to three pendula finding the smallest population condition for the chimera state.

This paper investigates the dynamical patterns in a new mechanical system composed by three identical, symmetric, pendulum-chart system. Dynamical patterns are classified, and a parametric analysis is developed establishing the main conditions to understand synchronization and chimera state. A novel energetic approach is proposed in order to define conditions for the different patterns including chimera state. The relation with natural frequencies and the chimera state is also pointed out. These novel approaches allow one to understand the main mechanisms that make the chimera state arises.

After this introduction, this paper is organized as follows. In Sect. 2, it is described the mechanical system and its mathematical model. A classification of dynamical patterns is also presented. Section 3 presents numerical simulations split into three subsections: parametric analysis; natural frequency analysis; energetic analysis. Section 4 presents the final remarks and conclusions.

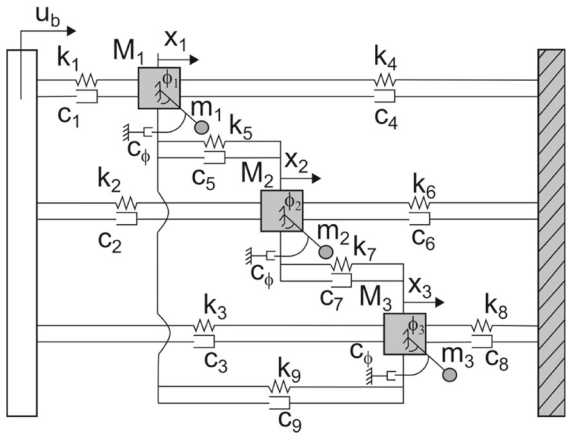

Fig. 1 Conceptual model of the coupled pendulum-chart system

2 Coupled pendulum-chart system

Consider a three coupled identical pendulum-chart system presented in Fig. 1. Each pendulum is connected to its own chart that is connected to the other charts through linear springs, and also to a rigid wall and to a base that provides harmonic excitation. Each chart has a mass M_i, and each pendulum is characterized by a length l and mass m_i ($i = 1, 2, 3$). Displacement x_i ($i = 1, 2, 3$) defines the chart displacement while angle ϕ_i ($i = 1, 2, 3$) measures the pendulum position. Linear springs, k_j ($j = 1, 2, \ldots, 9$), and linear viscous dampers, C_j ($j = 1, 2, \ldots, 9$), connect all oscillators in a symmetric way. Each pendulum has a linear viscous dissipation represented by coefficient C_ϕ. It should be pointed out that, due to symmetric coupling characteristics, any partial synchronization can be considered as a chimera state.

The equations of motion can be written considering Lagrange equations obtained from the kinetic and potential energies, resulting in the following set where it is adopted a harmonic basis excitation of the form $u_b = u \sin \Omega t$.

$$
\begin{aligned}
&(M_1 + m_1(1-\cos^2\phi_1))\ddot{x}_1 - \frac{C_\phi}{l}\dot{\phi}_1\cos\phi_1 \\
&\quad - m_1 g \sin\phi_1\cos\phi_1 - m_1 l\dot{\phi}_1^2\sin\phi_1 \\
&\quad + (C_1 + C_4 + C_5 + C_9)\dot{x}_1 - C_5\dot{x}_2 - C_9\dot{x}_3 \\
&\quad + (k_1 + k_4 + k_5 + k_9)x_1 - k_5 x_2 - k_9 x_3 \\
&\quad = uk_1 \sin\Omega t + uC_1\Omega\cos\Omega t \qquad (1)\\
&(M_2 + m_2(1-\cos^2\phi_2))\ddot{x}_2 - \frac{C_\phi}{l}\dot{\phi}_2\cos\phi_2 \\
&\quad - m_2 g \sin\phi_2\cos\phi_2 - m_2 l\dot{\phi}_2^2\sin\phi_2 \\
&\quad + (C_2 + C_5 + C_6 + C_7)\dot{x}_2 - C_5\dot{x}_1 - C_7\dot{x}_3 \\
&\quad + (k_2 + k_5 + k_6 + k_7)x_2 - k_5 x_1 - k_7 x_3 \\
&\quad = uk_2 \sin\Omega t + uC_2\Omega\cos\Omega t \qquad (2)\\
&(M_3 + m_3(1-\cos^2\phi_3))\ddot{x}_3 - \frac{C_\phi}{l}\dot{\phi}_3\cos\phi_3 \\
&\quad - m_3 g \sin\phi_3\cos\phi_3 - m_3 l\dot{\phi}_3^2\sin\phi_3 \\
&\quad + (C_3 + C_7 + C_8 + C_9)\dot{x}_3 - C_7\dot{x}_2 - C_9\dot{x}_1 \\
&\quad + (k_3 + k_7 + k_8 + k_9)x_3 - k_7 x_2 - k_9 x_1 \\
&\quad = uk_3 \sin\Omega t + uC_3\Omega\cos\Omega t \qquad (3)\\
&m_1 l^2\ddot{\phi}_1 + C_{\phi 1}\dot{\phi}_1 + m_1 g l\sin\phi_1 \\
&\quad + \frac{m_1 l\cos\phi_1}{(M_1 + m_1(1-\cos^2\phi_1))} \\
&\quad \times \left[\frac{C_\phi}{l}\dot{\phi}_1\cos\phi_1 + m_1 g\sin\phi_1\cos\phi_1\right. \\
&\quad + m_1 l\dot{\phi}_1^2\sin\phi_1 - (C_1 + C_4 + C_5 + C_9)\dot{x}_1 \\
&\quad + C_5\dot{x}_2 + C_9\dot{x}_3 - (k_1 + k_4 + k_5 + k_9)x_1 \\
&\quad \left. + k_5 x_2 + k_9 x_3 + uk_1\sin\Omega t + uC_1\Omega\cos\Omega t\right] \\
&\quad = 0 \qquad (4)\\
&m_2 l^2\ddot{\phi}_2 + C_{\phi 2}\dot{\phi}_2 + m_2 g l\sin\phi_2 \\
&\quad + \frac{m_2 l\cos\phi_2}{(M_2 + m_2(1-\cos^2\phi_2))} \\
&\quad \times \left[\frac{C_\phi}{l}\dot{\phi}_2\cos\phi_2 + m_2 g\sin\phi_2\cos\phi_2\right. \\
&\quad + m_2 l\dot{\phi}_2^2\sin\phi_2 - (C_2 + C_5 + C_6 + C_7)\dot{x}_2 \\
&\quad + C_5\dot{x}_1 + C_7\dot{x}_3 - (k_2 + k_5 + k_6 + k_7)x_2 \\
&\quad \left. + k_5 x_1 + k_7 x_3 + uk_2\sin\Omega t + uC_2\Omega\cos\Omega t\right] \\
&\quad = 0 \qquad (5)\\
&m_3 l^2\ddot{\phi}_3 + C_{\phi 3}\dot{\phi}_3 + m_3 g l\sin\phi_3 \\
&\quad + \frac{m_3 l\cos\phi_3}{(M_3 + m_3(1-\cos^2\phi_3))} \\
&\quad \times \left[\frac{C_\phi}{l}\dot{\phi}_3\cos\phi_3 + m_3 g\sin\phi_3\cos\phi_3\right. \\
&\quad + m_3 l\dot{\phi}_3^2\sin\phi_3 - (C_3 + C_7 + C_8 + C_9)\dot{x}_3 \\
&\quad + C_7\dot{x}_2 + C_9\dot{x}_1 - (k_3 + k_7 + k_8 + k_9)x_3 \\
&\quad \left. + k_7 x_2 + k_9 x_1 + uk_3\sin\Omega t + uC_3\Omega\cos\Omega t\right] \\
&\quad = 0 \qquad (6)
\end{aligned}
$$

Synchronization and chimera states can be elucidated by energy argues. In this regard, it is proposed a classification of the energy involved in the mechanical system. Basically, the potential energy of the elastic

springs and of the pendula are evaluated considering two groups: energy received from the base excitation, associated with springs k_1, k_2, k_3, k_4, k_6 and k_8; and energy transmitted either to the subsystems or to the movement, associated with springs k_5 k_7 and k_9, or the pendula. Therefore, it is possible to evaluate the energy through the charts, $E_{F,c}$,

$$E_{F,c} = \frac{1}{t}\int_0^t \left(\frac{k_5(x_2-x_1)^2 + k_9(x_3-x_1)^2}{k_1x_1^2 + k_4x_1^2} + \frac{k_5(x_2-x_1)^2 + k_7(x_3-x_2)^2}{k_2x_2^2 + k_6x_2^2} + \frac{k_7(x_3-x_2)^2 + k_9(x_3-x_1)^2}{k_3x_3^2 + k_8x_3^2} \right) \mathrm{d}t \tag{7}$$

And by the pendulum energy, $E_{F,p}$,

$$E_{F,p} = \frac{1}{t}\int_0^t \left(\frac{mgl(1-\cos\phi_1)}{k_1x_1^2 + k_4x_1^2} + \frac{mgl(1-\cos\phi_2)}{k_2x_2^2 + k_6x_2^2} + \frac{mgl(1-\cos\phi_3)}{k_3x_3^2 + k_8x_3^2} \right) \mathrm{d}t \tag{8}$$

The springs k_1, k_2 and k_3 receive energy from the base excitation that transmit this energy through the springs k_5, k_7 and k_9. When the excitation amplitude increases, the received energy increases as well. Energy accumulation tends to be greater close to the natural frequencies, and therefore, resonant conditions are situations with more energy accumulation.

2.1 Dynamical patterns

Dynamical patterns constitute an essential point for the synchronization analysis, and their definition needs a proper classification. In this work, six kinds of dynamical patterns are considered. For the sake of simplicity, this classification is explained considering three coupled oscillators, Fig. 2. The first two kinds of patterns are related to the classical definitions of synchronization, originally defined by Huygens [1]: in-phase synchronization (Fig. 2a) characterized by the same motion for all oscillators; and anti-phase synchronization (Fig. 2b), which occurs when one of the oscillators moves in opposite phase.

Other four different patterns are defined in the proposed classification. Frequency lock behavior (Fig. 2c) [2] is defined by variations of the orbit of one or more oscillators with respect to the synchronized group, presenting, however, the same frequency of the others,

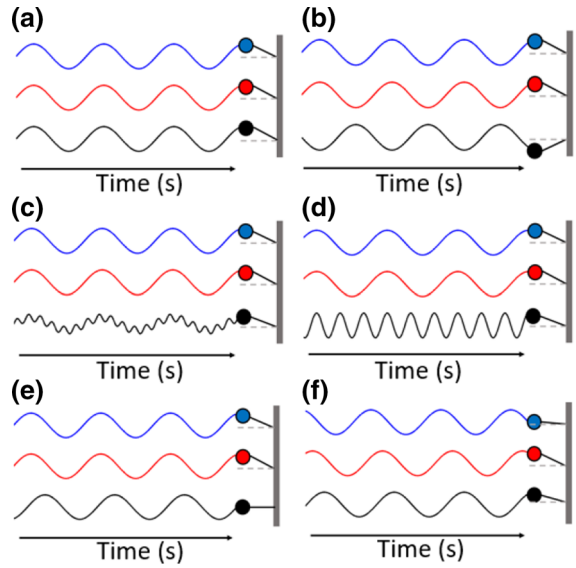

Fig. 2 Classification of the different kinds of dynamical patterns: **a** in-phase synchronization; **b** anti-phase synchronization; **c** frequency locked; **d** long period of synchrony; **e** chimera state; **f** desynchronized state

completing their orbits on the same instant. Long period synchronization (Fig. 2d) [3] is characterized by an oscillator with a frequency that is a multiple of the synchronized oscillators. Chimera state (Fig. 2e) [4] occurs when a partial synchronization occurs and therefore, an oscillator behaves independently and the others remain synchronized. Desynchronized behavior (Fig. 2f) is a situation where each oscillator moves independently from the others, without any pattern.

Based on these definitions of collective behavior, pattern classification can be done from time series analysis. The proposed procedure defines a difference-curve that is representative of the dynamical pattern. The first identification step is to define a reference, for example, the position of one of the oscillators, that is compared with the others. This comparison can be done by subtracting a signal with the reference. If this subtraction results in values close to zero for all the oscillators, the oscillators present in-phase synchronization. A second criterion can be verified when this is not satisfied, observing the sum of the subtracted signal by the double of the reference. If this sum is close to zero for at least one oscillator, the system presents an anti-phase synchronization.

A third verification criterion is established counting the peaks of the subtracted signal. When the distance

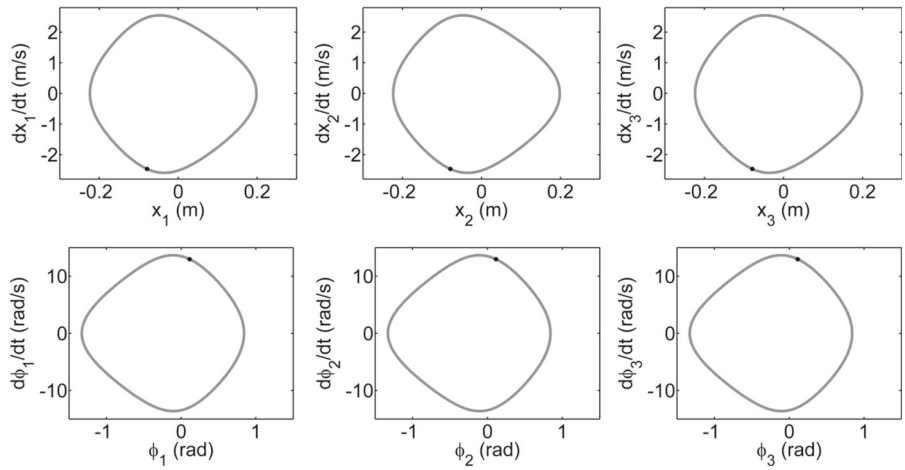

Fig. 3 Synchronized in-phase state—state spaces with $u = 1$ m, $\Omega = 10$ rad/s, $k_{1,2,3} = 20$ N/m and initial conditions with displacements $x_1 = x_2 = x_3 = 1$ m

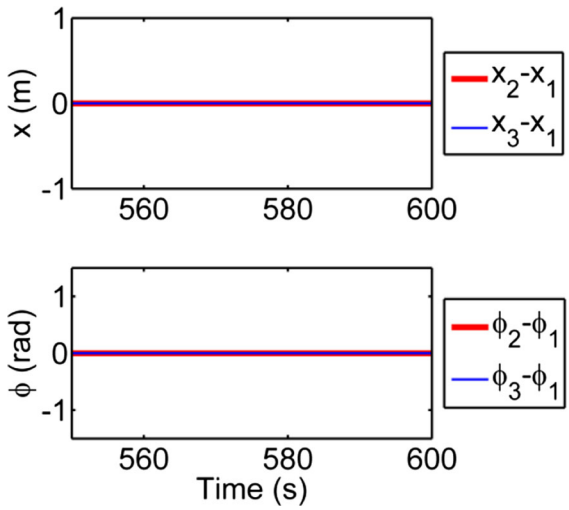

Fig. 4 Difference-curves for the periodic synchronized behavior

of subsequent peaks is the same, the system presents a frequency locked behavior. Otherwise, when the distances are different, the system presents a long period of synchrony.

After the verification of these criteria, if the response is not properly classified, the reference oscillator is changed and all the process is repeated. If this reference change allows the classification of a synchrony behavior, the system response is classified as chimera state. Afterward, if none of these patterns is identified, the reference oscillator is changed again. After the verification of all oscillators as reference, if none of these patterns is identified, the system is classified as desynchronized.

3 Numerical simulations

Synchronization analysis is investigated by considering numerical simulations developed with the fourth order Runge–Kutta method. Lyapunov exponents are employed to evaluate the chaotic behavior, being estimated using the algorithm due to Wolf et al. [60]. Basically, the six dynamical patterns defined are of concern: in-phase synchronization, anti-phase synchronization, frequency locked, long period synchronization, chimera state and desynchronized state.

The following parameters are adopted: $k_{4,6,8} = 0$ N/m, $k_{5,7,9} = 50$ N/m, $g = 9.81$ m/s^2, $l = 0.2$ m, $M = 1$ kg, $m = 1$ kg, $C_{1,2,3,5,7,9} = 0.56$ Ns/m, $C_{4,6,8} = 0$ Ns/m, $C_\phi = 0.01$ Ns/m. Initial conditions of the pendula always vanish velocity and displacement. Parameters $k_{1,2,3}$, u, Ω and the initial conditions of the charts are altered according the situations.

Initially consider $u = 1$ m, $\Omega = 10$ rad/s, $k_{1,2,3} = 20$ N/m and initial conditions $x_1 = x_2 = x_3 = 1$ m that produces a period-1 in-phase synchronized response presented in the form of phase space and Poincaré maps in Fig. 3, considering subspaces related to each chart and each pendulum. The dynamical pattern analysis is represented by difference-curves that establish the criterion for pattern classification, Fig. 4.

By considering $k_{1,2,3} = 20$ N/m and initial conditions with null displacement to all charts, the system presents a synchronized chaotic behavior, Fig. 5. Lyapunov exponents assure this behavior, presenting a positive greatest value, 0.66, which confirms the existence of chaos. The difference-curves confirm the synchronized behavior presenting a constant null value, Fig. 6.

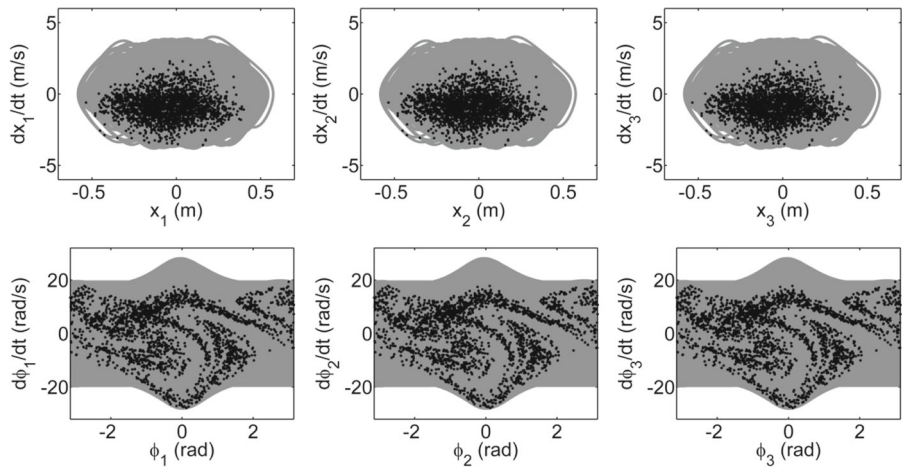

Fig. 5 Synchronized chaotic behavior—state spaces with $u = 1$ m, $\Omega = 10$ rad/s, $k_{1,2,3} = 19$ N/m and initial conditions $x_1 = x_2 = x_3 = 0$ m

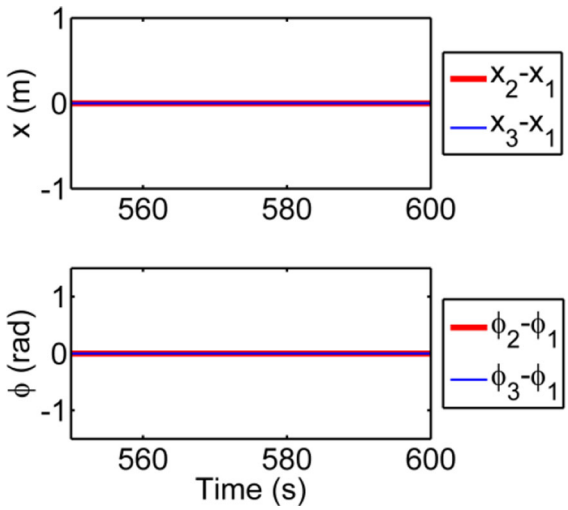

Fig. 6 Difference-curves for the synchronized chaotic behavior

A desynchronized state is reached assuming $u = 0.2$ m, $\Omega = 9.1$ rad/s, $k_{1,2,3} = 19.1$ N/m and initial conditions with $x_1 = 1$ m and null displacements to the other charts. Figure 7 shows a desynchronized chaotic response, with the highest Lyapunov exponent of 0.87, where it is noticeable that either the charts or the pendula exhibit similar state space and Poincaré map, Fig. 7. This is a consequence of similar responses but with independent motion, as can be observed by the difference-curves of Fig. 8 with an evident discrepancy. Thereby, the oscillators move in an independent way and it is not possible to identify any of the dynamical patterns.

The chimera state is reached when $u = 1$ m, $\Omega = 9$ rad/s, $k_{1,2,3} = 20$ N/m and initial conditions $x_1 = x_3 = 1$ m and $x_2 = 0$, Fig. 9. Note that the second pendulum-chart response is different from the others and this chimera state is associated with a

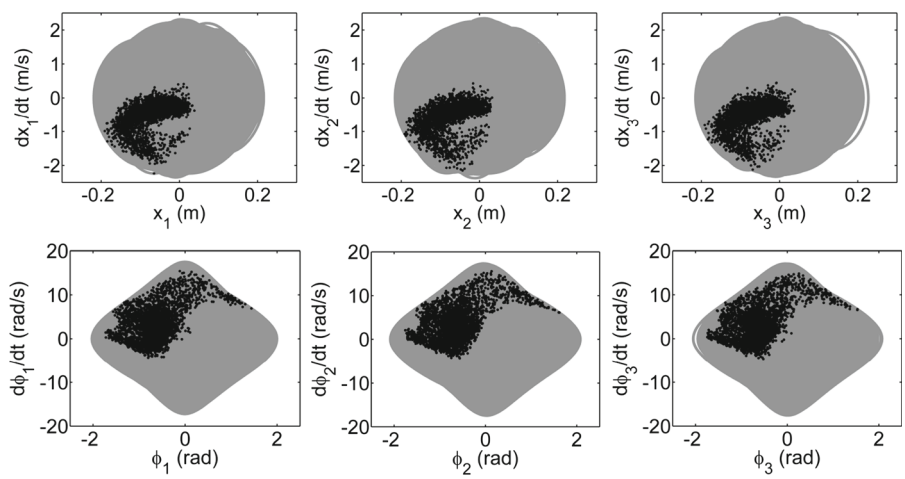

Fig. 7 Desynchronized state—state spaces with $u = 0.2$ m, $\Omega = 9.1$ rad/s, $k_{1,2,3} = 19.1$ N/m and initial condition $x_1 = 1$ m and null displacement to the other charts

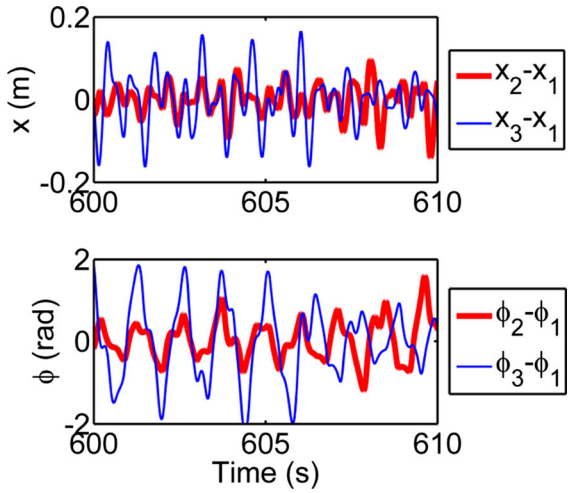

Fig. 8 Difference-curves for the desynchronized behavior

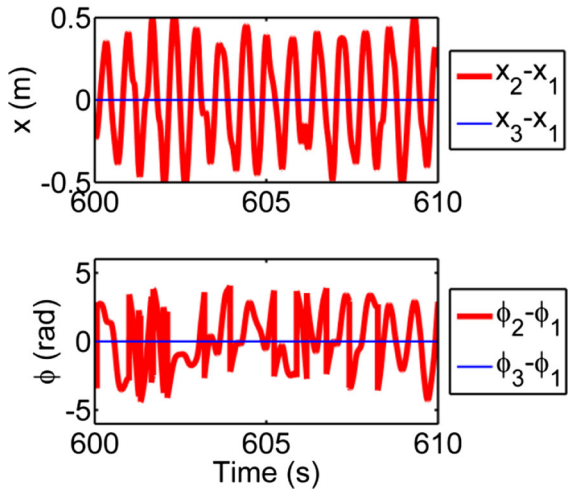

Fig. 10 Difference-curves for the chimera state

hyperchaotic motion characterized by two positive Lyapunov exponents, 0.89 and 0.40. Difference-curves confirm this observation showing a null difference for the first and third systems and a different response for the second one (Fig. 10).

Frequency lock synchronization is obtained by assuming parameters of $u = 0.5$ m, $\Omega = 9.9$ rad/s, $k_{1,2,3} = 13.5$ N/m and initial conditions with $x_1 = 1$ m and null displacement of the others charts, Fig. 11. The first pendulum-chart system oscillates in a different orbit compared with the other two systems. The difference-curves show that the third and second oscillators have similar curves, showing that the first pendulum-chart moves in a different manner while the others are synchronized, Fig. 12. However, as the periodicity of the signal indicates, there is a pattern between the oscillators. Figure 13 presents a time history of each oscillator response showing that they are on the same frequency even with different amplitudes, which characterize the frequency lock synchronization.

By assuming $u = 0.2$ m, $\Omega = 11$ rad/s, $k_{1,2,3} = 16.6$ N/m and initial conditions with $x_1 = 1$ m and null displacement to the others charts, Fig. 14 exhibits in-phase synchronized behavior to the charts and anti-phase synchrony for the pendula, which is observed from the position of the Poincaré section that presents a single point in a symmetric position from others with respect to y-axis. Difference-curves show that charts have synchronized response and the second and the third pendula are similar with respect to the first pendu-

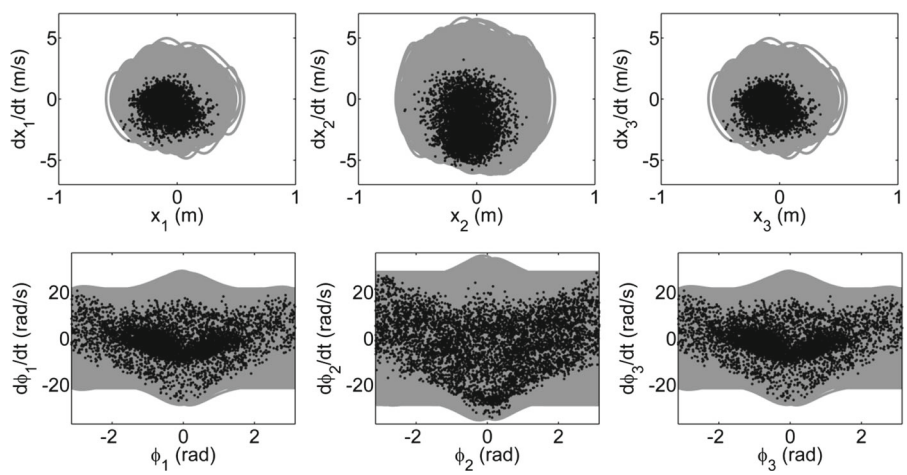

Fig. 9 Chimera state associated with hyperchaos-state spaces with $u = 1$ m, $\Omega = 9$ rad/s, $k_{1,2,3} = 20$ N/m and initial condition $x_1 = x_3 = 1$ m and $x_2 = 0$

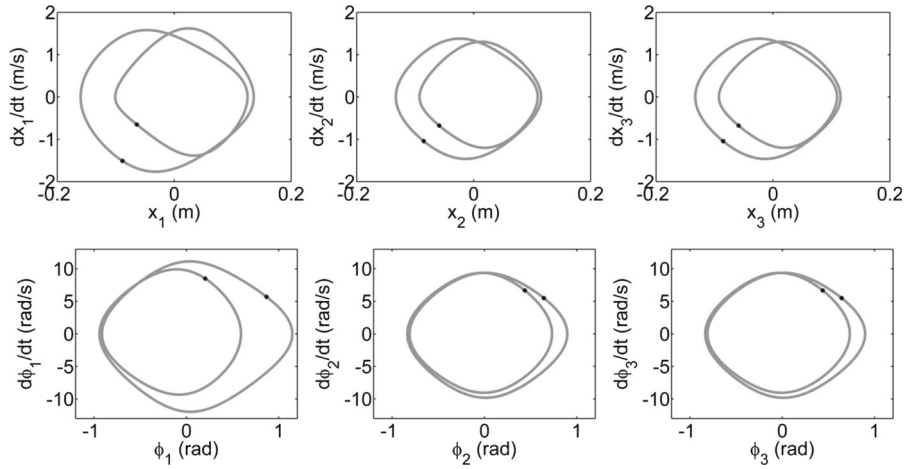

Fig. 11 Frequency lock behavior—state spaces with $u = 0.5\,\text{m}$, $\Omega = 9.9\,\text{rad/s}$, $k_{1,2,3} = 13.5\,\text{N/m}$ and initial condition $x_1 = 1\,\text{m}$ and null displacement to the others charts

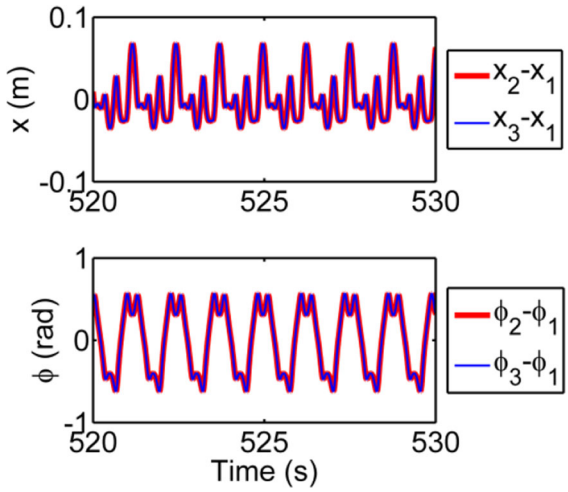

Fig. 12 Difference-curves of the frequency lock behavior

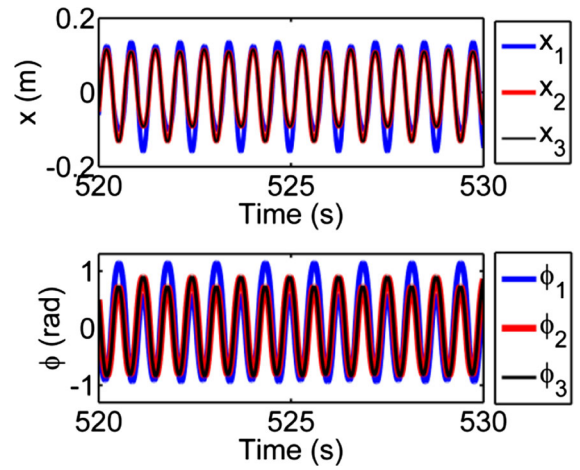

Fig. 13 Frequency lock behavior time history

lum, Fig. 15. The anti-phase characteristic is observed from time history, Fig. 16, where it is possible to observe that the difference of positions provides the double of the amplitude of response. Moreover, the sum of this difference signal to the double of the original reference response results vanishes, satisfying the criterium and allowing the classification of this response.

Long period of synchronization is discussed considering $u = 0.2\,\text{m}$, $\Omega = 9.5\,\text{rad/s}$, $k_{1,2,3} = 6.5\,\text{N/m}$ and initial conditions with $x_1 = 1\,\text{m}$ and null to the other charts, Fig. 17. It is noticeable that the first pendulum-chart moves in quasiperiodic motion characterized by a closed curve Poincaré section and confirmed by a null Lyapunov exponent.

Difference-curves exhibit two similar curves showing the synchrony between the second and third oscillators, Fig. 18. The long period of synchronization can be observed counting the peaks and comparing the repeating of the signal, as presented in Fig. 19 that shows two dashed line boxes illustrating the long period of the system exhibiting the same curve.

3.1 Parametric analysis

A parametric analysis is developed in this section in order to elucidate the different patterns and the transition among them. In this regard, it is plotted pattern diagrams representing the classified dynamical patterns on the parameter domain. The procedure is similar to a basin of attraction, identifying each steady-state pattern on the parameter domain based in the process described in Sect. 2.1, established based on

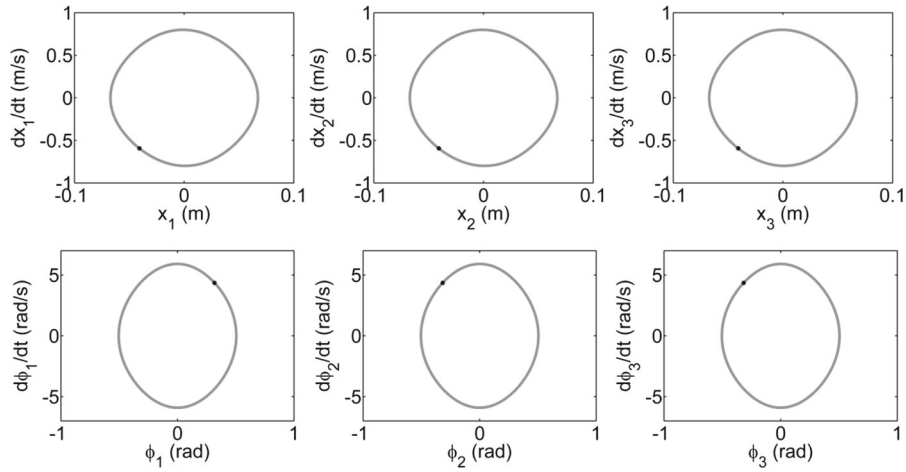

Fig. 14 Anti-phase synchronization—state spaces with $u = 0.2$ m, $\Omega = 11$ rad/s, $k_{1,2,3} = 16.6$ N/m and initial condition $x_1 = 1$ m and null displacement to the others charts

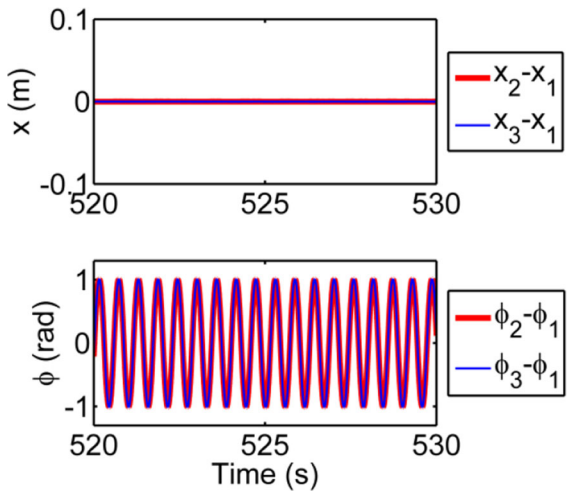

Fig. 15 Difference among charts and pendula in anti-phase synchronized behavior

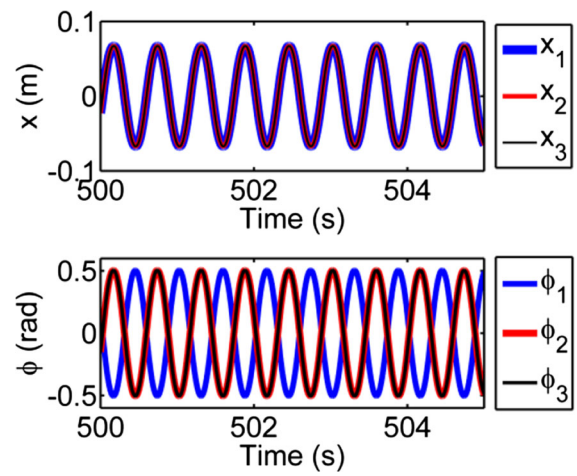

Fig. 16 Anti-phase behavior represented by time series with $u = 0.2$ m, $\Omega = 11$ rad/s, $k_{1,2,3} = 16.6$ N/m and initial condition $x_1 = 1$ m and null displacement to the others charts

the oscillator time series. In addition, different diagrams are presented showing chart responses, pendulum responses and pendula-charts responses. Parametric space is defined by the excitation frequency and spring coefficients that connect the charts to base excitation, assumed to be equal, $k = k_1 = k_2 = k_3$.

Figure 20 presents the chart pattern diagram for different values of excitation amplitudes identifying the dynamical patterns. Diagram presents a big region related to in-phase synchronized behavior (gray) and a region with desynchronized and chimera state, with few frequency locked points, named as the asynchronous region. Despite this name, it is important to note that there are some points related to frequency locked behavior that, as a matter of fact, is a synchronized behavior. This asynchronous region tends to increase with the increase in excitation amplitude as observed comparing Fig. 20a–d. Figure 20a shows the response to an amplitude of $u = 0.1$ m. By changing to an amplitude $u = 0.2$ m, Fig. 20b, a second asynchronous region emerges close to 3 rad/s. It is also noticeable that desynchronized behavior increases. Figure 20c considers an amplitude of $u = 0.5$ m and the asynchronous bandwidth around 10 rad/s becomes even larger and the second band in 3 rad/s increases its length. The desynchronized response has a stronger presence with $u = 0.5$ m and there are new areas with the chimera behavior mainly around 20 rad/s, expanding the asynchronous region. Finally, by considering an amplitude excitation of $u = 1$ m, Fig. 20d, response trend is even

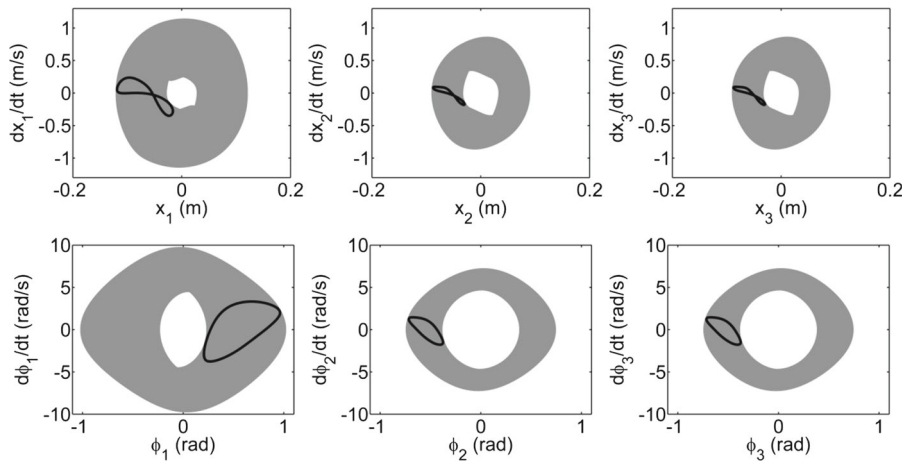

Fig. 17 Long period synchronization—state spaces $u = 0.2$ m, $\Omega = 9.5$ rad/s, $k_{1,2,3} = 6.5$ N/m and initial conditions $x_1 = 1$ m and null displacement to the others charts

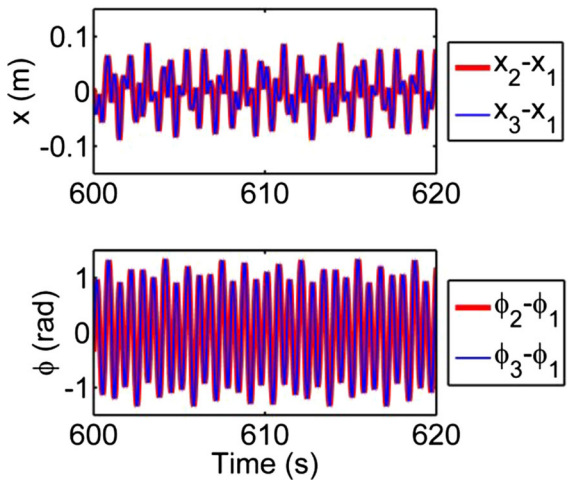

Fig. 18 Difference-curves for the long period of synchronization

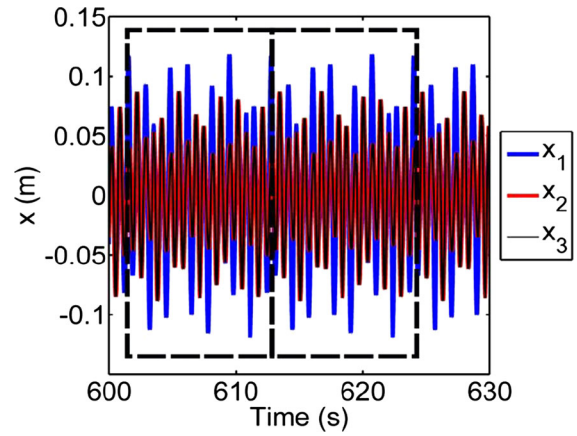

Fig. 19 Long period synchronization time history for the parameters of $u = 0.2$ m, $\Omega = 9.5$ rad/s, $k_{1,2,3} = 6.5$ N/m and initial condition $x_1 = 1$ m and null displacement to the others charts. In the dashed line box is the long period of synchrony

more evident but there is a new trend to spread this behavior in a more diffuse way. These results show a strong dependency of the asynchronous region to the excitation amplitude. That is, an increase in the amplitude has, as a consequence, a larger asynchronous band.

The same diagrams are now built for the pendula, Fig. 21. The same trends are observed for the asynchronous region. Nevertheless, the synchronized region is altered presenting a complex structure between in-phase and anti-phase patterns (dark-gray and gray regions). The borders between in-phase and anti-phase present a complex pattern, sometimes with fractal-like characteristics. For the increase in the amplitude excitation to $u = 0.2$ m, asynchronous band shows again the same borders presented in Fig. 20b. In Fig. 21b the desynchronized behavior concentrated to higher values of stiffness when compared to the chart analysis, Fig. 20b, where the chimera and desynchronized behaviors are more mixed. By observing Fig. 21c, d, respectively, associated with amplitude of 0.5 and 1 m, the areas where the chimera behaviors are observed are the same of the charts analysis to the same amplitudes. Nevertheless, the pendulum ensembles have desynchronized state more concentrated than the charts, and the structure between in-phase and anti-phase behaviors becomes even more complex and diffuse with the increase in the amplitude.

By analyzing together both charts and pendula, Fig. 22, it is noticeable the same trends, especially the asynchronous region. Nevertheless, it is important to observe that the form of synchronization is different since six oscillators are of concern, instead of three.

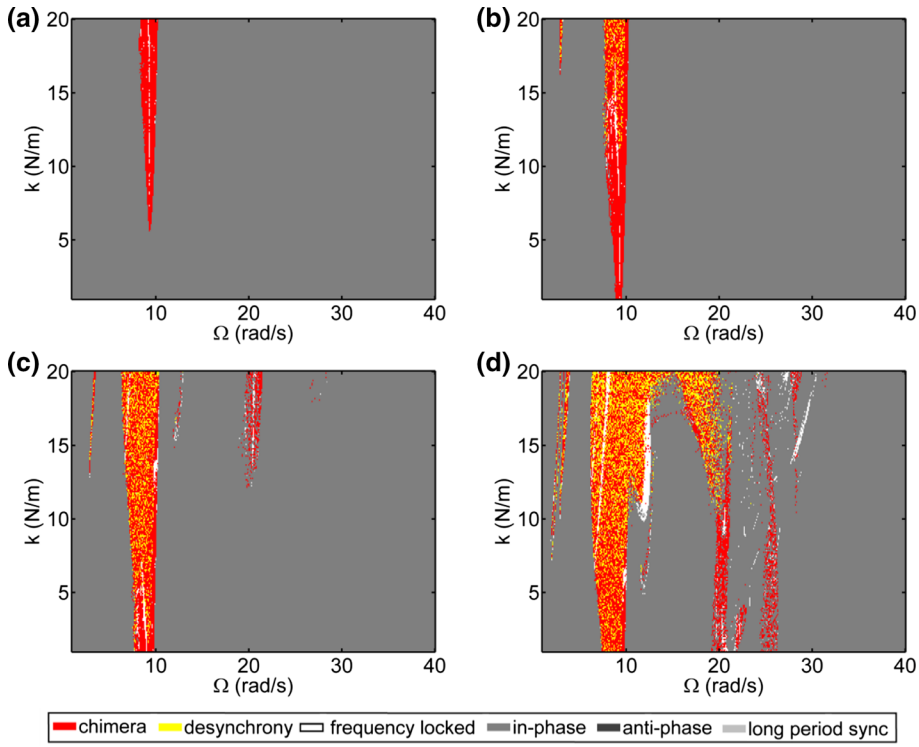

Fig. 20 Pattern diagram of the charts for different excitation amplitudes: **a** $u = 0.1$ m; **b** $u = 0.2$ m; **c** $u = 0.5$ m; **d** $u = 1$ m

Thereby, even when pendula and charts are synchronized, it is possible that each subgroup is not synchronized to each other. Based on that, some synchronized behaviors appear as frequency locked when evaluated together. Furthermore, the asynchronous region remains with the same border. The desynchronized state of Fig. 22 corresponds just to the points that this pattern is identified for both pendula and charts, Figs. 20 and 21.

Martens et al. [6] proposed a hypothesis where chimera state is a consequence of the competition between in-phase and anti-phase synchronized behaviors. Basically, chimera state is propitious to occur between these synchronization regions. By observing the pendulum pattern diagram it is clear that, for low energy excitation ($u = 0.1$ m), the hypothesis seems to be an interesting explanation about the transition for some areas, Fig. 23b. This area shows the same transition from in-phase to anti-phase of the competition hypothesis. Nevertheless, other areas presented in Fig. 23c show that the in-phase behavior appears in both sides of the chimera behavior, outside the limits between in-phase and anti-phase. Thereby, considering the competition hypothesis, the chimera state should emerge just in the transition from one pattern to the other. However, the asynchronous region shape is not related to the fractal-like distribution between in-phase and anti-phase, even to higher amplitudes excitation, where this form becomes more complex.

Furthermore, the increase in the asynchronous region for higher excitation amplitude is not related to a possible competition of patterns. This correlation indicates a dependency to the level of energy in the system, meaning that the increase in the excitation amplitude promotes the growth of the asynchronous areas.

3.2 Natural frequency analysis

Further the competition hypothesis, chimera state was associated with system natural frequencies in different references [6,7]. This section treats an analysis of natural frequencies, considering a linearized approach. Basically, governing equations (1–6) are linearized by assuming $\sin\phi_i \approx \phi_i$, $\cos\phi_i \approx 1$ and $\dot{\phi}_i^2 \sin\phi_i \approx 0$. Based on that, three different analyses are performed: charts-pendula; charts; and pendula. The first two cases

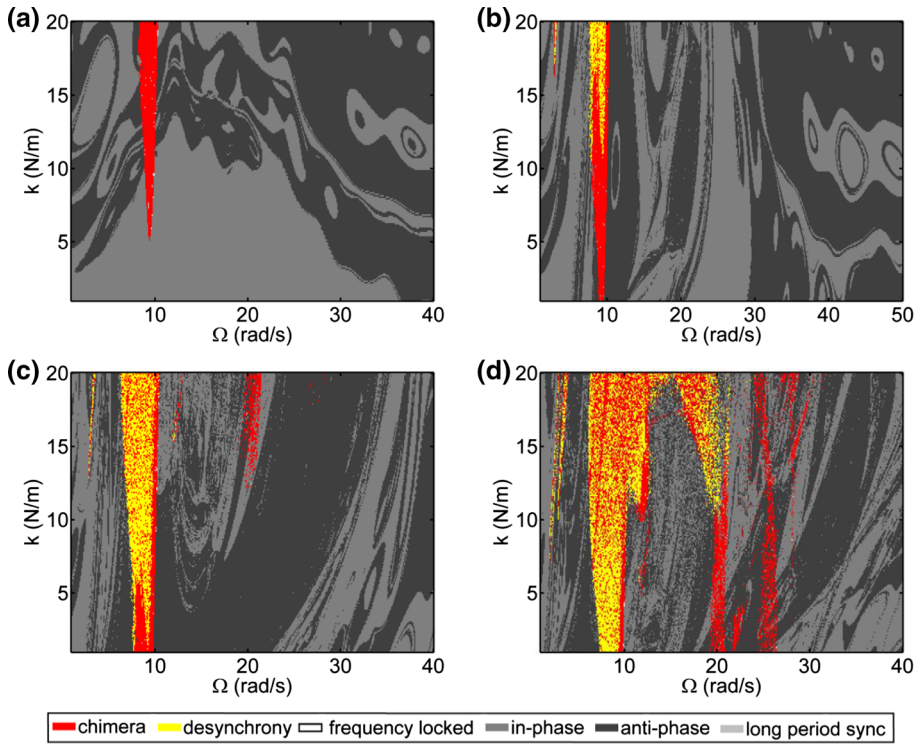

Fig. 21 Pattern diagram for different excitation amplitudes: **a** $u = 0.1$ m; **b** $u = 0.2$ m; **c** $u = 0.5$ m; **d** $u = 1$ m

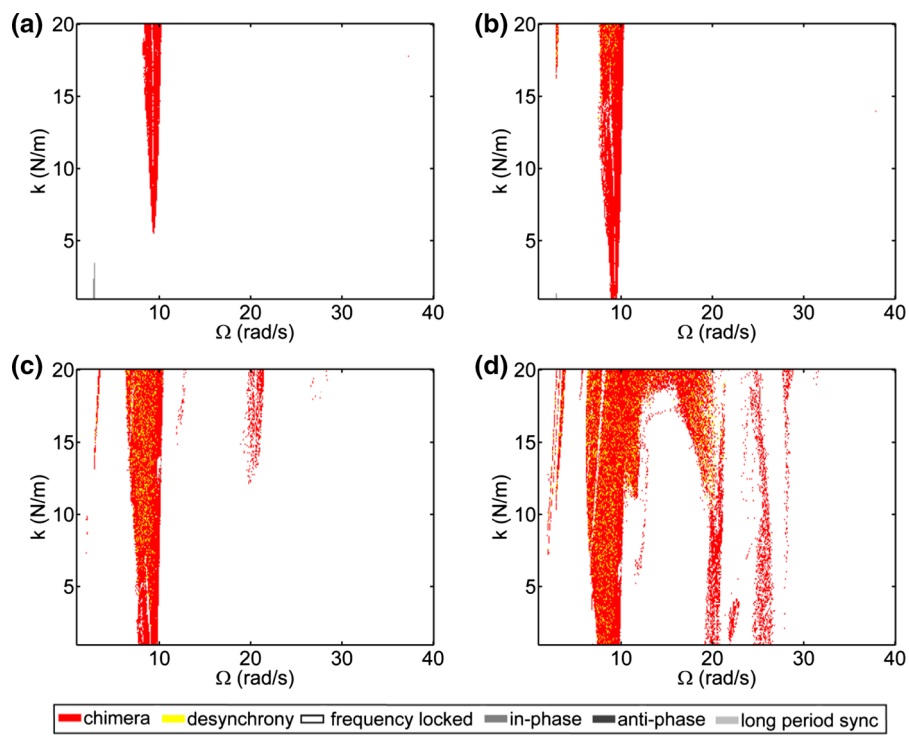

Fig. 22 Complete pattern diagram combining charts and pendula for different excitation amplitudes: **a** $u = 0.1$ m; **b** $u = 0.2$ m; **c** $u = 0.5$ m; **d** $u = 1$ m

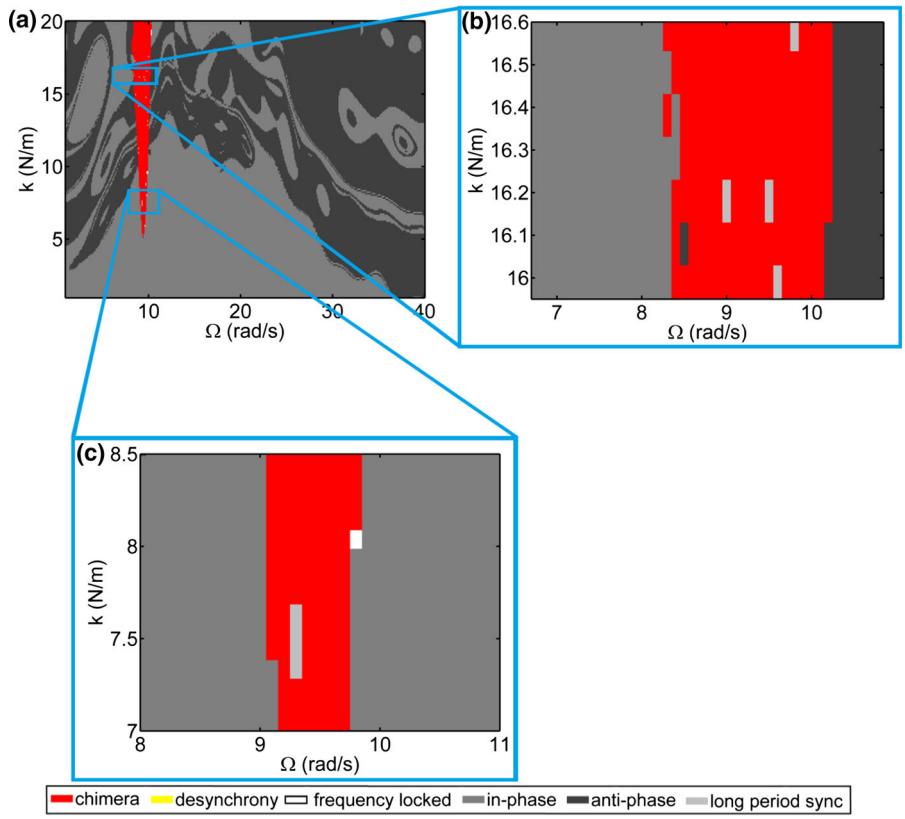

Fig. 23 Pendulum pattern diagram with $u = 0.1$ m: **a** complete diagram; **b** zoom with chimera state between in-phase and anti-phase synchronizations; **c** zoom with chimera state between in-phase synchronization regions

are analyzed from the eigenvalues of the linearized system. The third case is the isolated linearized pendulum frequency. Results of this analysis are presented in Fig. 24 together with the pattern diagram of Fig. 21b. Blue lines represent the natural frequencies of the linearized pendulum-chart system; green lines represent the chart system; cyan lines represent the isolated pendulum response. Note that some of these linearized frequencies, in blue, are related to the borders of the asynchronous region following the same contour trend of the asynchronous region.

Another analysis related to resonant conditions is developed considering amplitude response, building a curve of the maximum steady-state amplitude to each value of frequency, using the same initial conditions. This curve presents peaks around the natural frequencies allowing the identification of nonlinear resonant conditions. Figure 25 presents results for an amplitude excitation $u = 0.2$ m and $k_{1,2,3} = 20$ N/m, related to a horizontal cut of Fig. 24 at 20 N/m. The frequencies of the linearized system in represented in blue, the charts in green and the pendulum in cyan. The system shows two peaks of chart displacement at frequencies 3 rad/s and 8 rad/s, Fig. 25. Note that there is a correlation between the peak and the asynchronous region. The asynchronous region is close to dynamical jump, around 10 rad/s, and also close to the peak of 3 rad/s. The amplitude response shows a close relation with natural frequencies obtained by linearization, blue lines. The first blue line fits the first peak and the other three surrounds the jump phenomenon. Based on that, it is possible to confirm the relation between the chimera state and the natural frequencies of the system.

3.3 Energetic analysis

Results of the previous analysis indicate that either chimera state or desynchronized responses are related to natural frequencies. For instance, Figs. 20, 21 and 22 show that the increase in the excitation amplitude causes the increase in the asynchronous region that contains the chimera state. This observation can be explained by energetic argues since the bigger is the excitation amplitude, the higher is the energy supplied

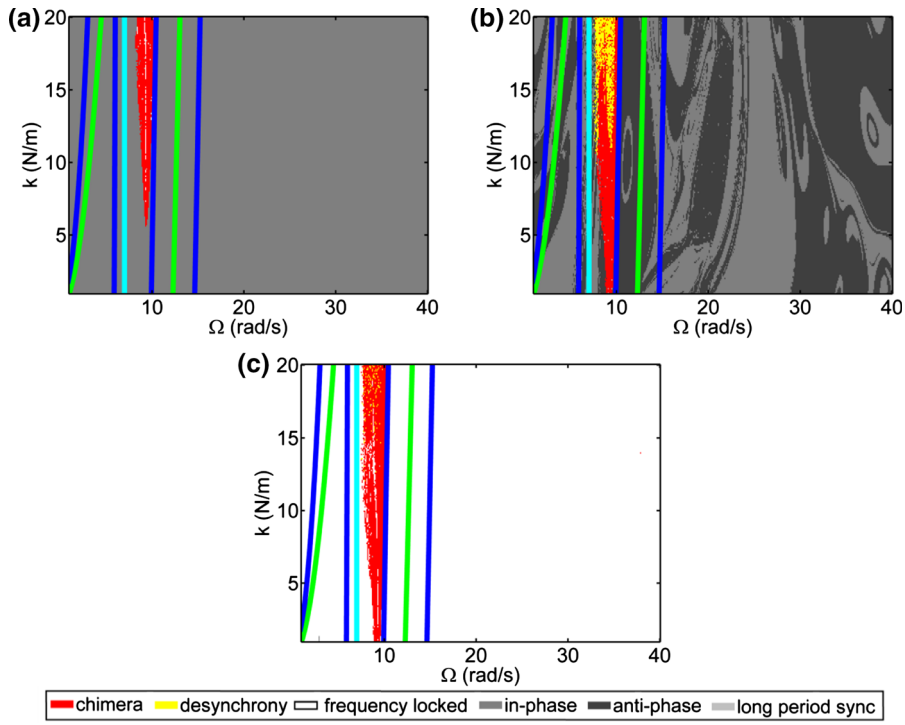

Fig. 24 Linearized natural frequencies analysis over the pattern diagram with $u = 0.2$ m. Blue lines represent the linearized natural frequencies of the chart-pendulum system; green lines represent natural frequencies of the charts; cyan represents natural frequencies of the pendulum. **a** Chart diagram. **b** Pendulum diagram. **c** Complete chart-pendulum diagram

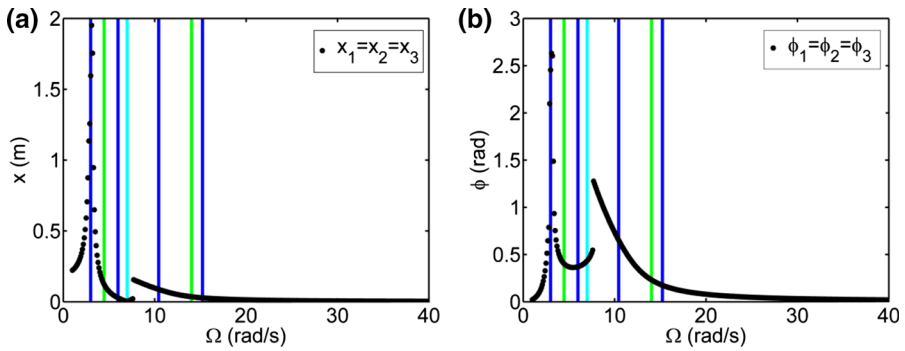

Fig. 25 Frequency response with $u = 0.2$ m and $k_{1,2,3} = 20$ N/m and initial conditions of null displacements and velocities. Curves are plotted together with linearized natural frequencies. Blue lines represent the linearized natural frequencies of the chart-pendulum system; green lines represent natural frequencies of the charts; cyan represent natural frequencies of the pendulum

to the system. This section employs energetic argues to establish conditions for chimera and asynchronous states.

Based on that, it is proposed a hypothesis that the chimera state comes from the accumulation of energy, which is transmitted through the populations. Note that springs k_1, k_2 and k_3 receive energy from the base excitation that, in turn, transmit energy through the springs k_5, k_7 and k_9. Therefore, the increase in the excitation amplitude increases the energy received. When the transmission capacity overcomes the amount received, either chimera or desynchronized state appears (Figs. 20, 21, 22). This behavior is observed close to the natural frequencies, as can be observed in Fig. 25. Thereby, chimera and desynchronized states emerge in situations close to resonance or jump phenomenon, where the system accumulates more energy.

Figure 26 shows an energetic diagram for the charts using the definitions presented in Eq. 7, using a loga-

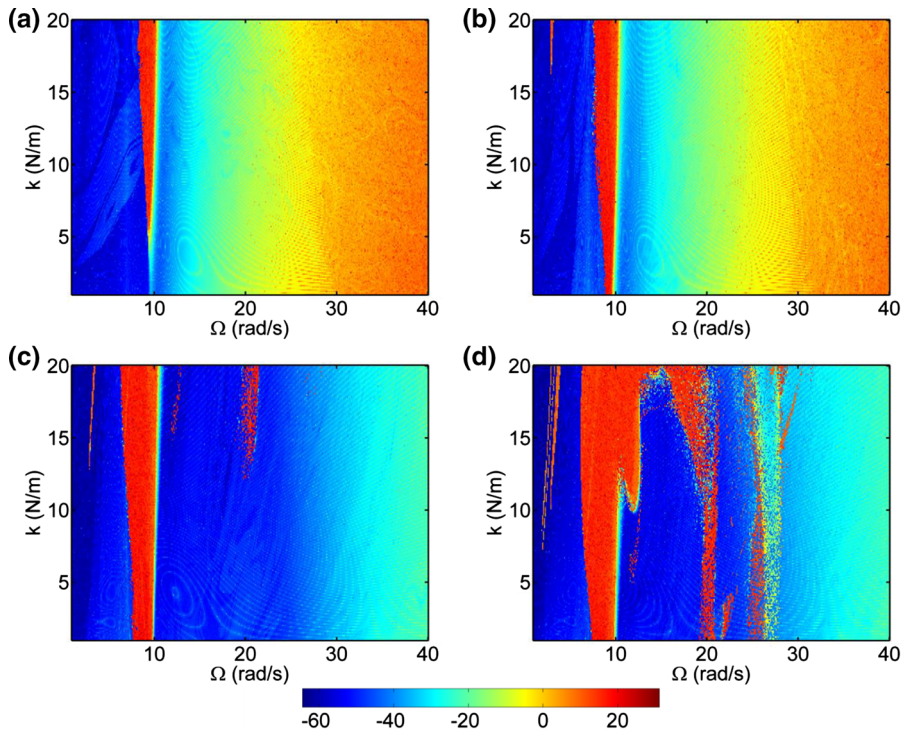

Fig. 26 Energetic diagram in logarithmic scale considering the chart springs and different excitation amplitudes: **a** $u = 0.1$ m; **b** $u = 0.2$ m; **c** $u = 0.5$ m; **d** $u = 1$ m

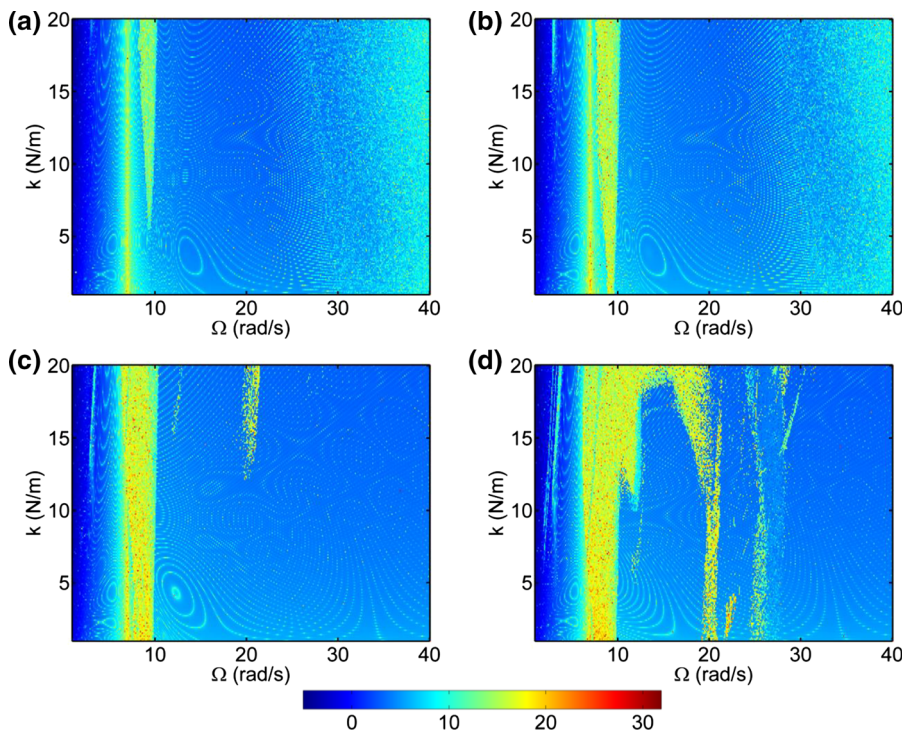

Fig. 27 Energetic diagram in logarithmic scale considering the pendula and different excitation amplitudes: **a** $u = 0.1$ m; **b** $u = 0.2$ m; **c** $u = 0.5$ m; **d** $u = 1$ m

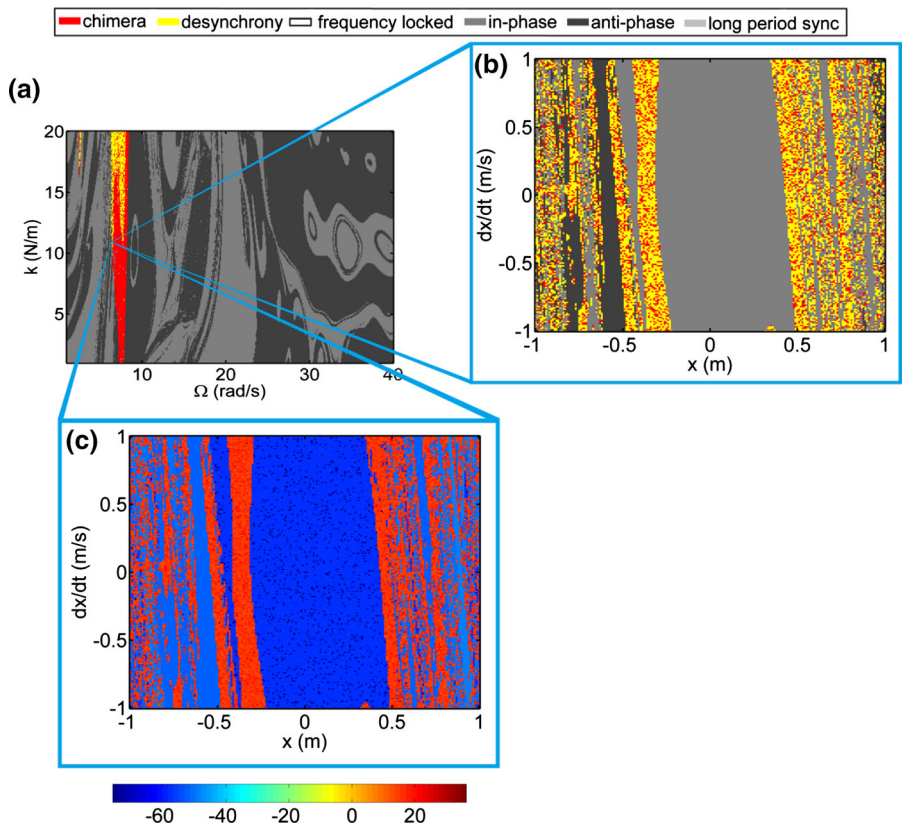

Fig. 28 Pattern diagram analyzing initial conditions for the pendula with $u = 0.2$ m, $\Omega = 7.7$ rad/s, and $k_{1,2,3} = 10.8$ rad/s. **a** Complete pattern diagram; **b** pattern diagram; **c** energetic diagram

rithm scale. It should be pointed out that high energy values are concentrated in the asynchronous region. Figure 27 shows the same energetic diagram considering the pendulum system using the definition of Eq. 8. The same trend is observed; nevertheless, it is noticeable that the energy level is lower when compared with the charts. It is also observed that around 7 rad/s, there is a higher energy band that is not observed on the chart diagram (Fig. 26). This behavior is not due the asynchronous region, instead it is a consequence of the natural frequency of the pendulum ensemble, as observed in Fig. 24, the cyan line.

Comparing Fig. 26 with Fig. 27 and considering the asynchronous region exhibited in Figs. 20, 21 and 22, it is noticeable that the chart energetic diagram (Fig. 26) is a better representation of the dynamical patterns.

The influence of initial conditions is now investigated by considering pattern diagrams on the initial condition space. By considering the parameters $u = 0.2$ m , $\Omega = 7.7$ rad/s and $k_{1,2,3} = 10.8$ rad/s, Fig. 28a presents pattern diagram of the pendulum systems and the influence of initial conditions is analyzed in Fig. 28b. Fractal structures appear between the in-phase and anti-phase behaviors. Figure 28c shows the energetic diagram on the same space, showing the distinction between the synchronous and the asynchronous patterns. Once again, the increase in energy level tends to be effective to generate asynchronous behavior. Note that there is a larger amount of asynchronous behavior associated with initial conditions far from the origin.

A classical measure of synchronization is provided by the order parameter of Kuramoto [6,8,9]. This parameter is given by $Z = N^{-1}\sum_{p=1}^{N} e^{i\theta}$, where N is the number of oscillators and θ is the phase on state space. This parameter quantifies the synchrony of a group of oscillators, being zero to the desynchronized state and one to the synchronized state. Figure 29 shows the Kuramoto parameter using the following conditions: $u = 0.2$ m and initial conditions $x_1 = 1$ m and null to the others, the same conditions of Fig. 21b. Different diagrams are plotted considering the three situations: charts; pendula; and complete pendulum-chart system. Figure 29a shows the order parameter of

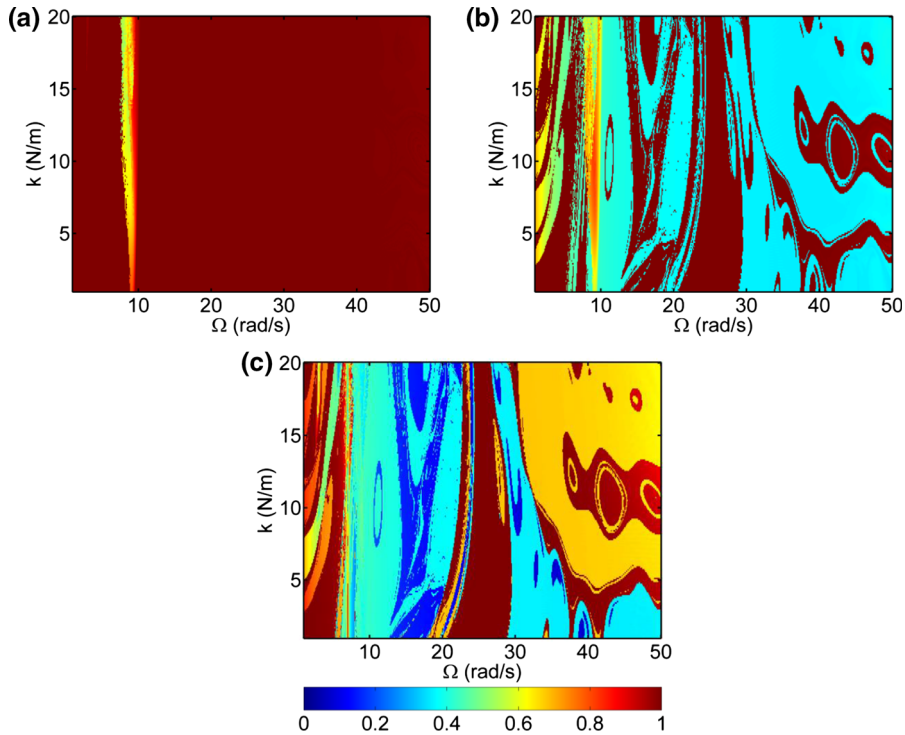

Fig. 29 Order parameter of Kuramoto (Z) with $u = 0.2$ m: **a** charts; **b** pendula; and **c** complete chart-pendulum system

Kuramoto for the charts. Figure 29b shows the pendulum system, and Figure 29c presents the complete system considering the pendula-charts. Figure 29a points a similar structure presented by considering dynamical pattern and energetic diagrams, showing the asynchronous region. The same occurs for the pendulum system, Fig. 29b, where a complex structure appears out of the asynchronous region that presents in-phase and anti-phase synchronization. Figure 29c has a similar structure where it is possible to identify the asynchronous region and the complex structure expressing the different kinds of patterns. Nevertheless, it should be pointed out that the Kuramoto's index does not allow a proper classification of the different kinds of patterns.

4 Conclusions

This paper deals with synchronization and chimera state of a mechanical system composed by three chart-pendulum oscillators symmetrically coupled. Dynamical patterns are classified considering six kinds of responses: in-phase synchronization, anti-phase synchronization, frequency locked, long period synchronization, chimera state and desynchronized state. The classifications are performed from time series analysis that allows the use of difference-curves to observe the system response. Based on this classification, a parametric analysis is carried out employing pattern diagrams on parameter domain. Numerical simulations point that asynchronous behavior is related to high level of energy that induces symmetry break. This argue motivates the analysis of natural frequencies. Resonance conditions is propitious for this due high energy scenario. An energetic approach is proposed to evaluate the synchronization. It confirms that synchronization is a natural state of the system and its break needs a high level of energy. Although useful together with pattern analysis, the energetic approach does not establish the required level for pattern break.

Acknowledgements The authors would like to acknowledge the support of the Brazilian Research Agencies CNPq, CAPES and FAPERJ.

Funding Funding was provides by Coordenação de Aperfeiçoamento de Pessoal de Nível Superior, Conselho Nacional de Desenvolvimento Científico e Tecnológico and Fundação Car-

los Chagas Filho de Amparo à Pesquisa do Estado do Rio de Janeiro.

Compliance with ethical standards

Conflict of interest The authors declare that they have no conflict of interest.

References

1. Huygens, C.: L'Horloge à pendule de 1651 à 1666. Travaux divers de physique, de mécanique et de technique de 1650 à 1666. Traité des couronnes et des parhélies (1662 ou 1663), vol. 17. Swets & Zeitlinger N. V., Amsterdam (1666)
2. Huygens, C.: Correspondance 1664–1665, vol. 5. Société Hollandaise des sciences, Amsterdam (1665)
3. Kapitaniak, M., Czolczynski, K., Perlikowski, P., Stefanski, A., Kapitaniak, T.: Synchronization of clocks. Phys. Rep. **517**, 1–69 (2012). https://doi.org/10.1016/j.physrep.2012.03.002
4. Bennett, M., Schatz, M.F., Rockwood, H., Wiesenfeld, K.: Huygens' s clocks. Proc. R. Soc. Lond. A **458**, 563–79 (2002). https://doi.org/10.1098/rspa.2001.0888
5. Buck, J., Buck, E.: Mechanism of rhythmic synchronous flashing of fireflies. Science **159**, 1319–27 (1968). https://doi.org/10.1126/science.159.3821.1319
6. Ravasz, E., Néda, Z., Vicsek, T., Brechet, Y., Barabási, A.L.: Physics of the rhythmic applause. Phys. Rev. E **61**, 6987–92 (2000). https://doi.org/10.1007/BF02068742
7. Walker, T.J.: Acoustic synchrony: two mechanisms in the snowy tree cricket. Science **166**, 891–4 (1969). https://doi.org/10.1126/science.166.3907.891
8. Wiener, N.: Nonlinear Problems in Random Theory. MIT Press, Cambridge (1958)
9. Wiener, N.: The human use of human beings: cybernetics and society, vol. 20. Free Association Books, London (1989). https://doi.org/10.1109/TIT.1974.1055201
10. Winfree, A.T.: Biological rhythms and the behavior of populations of coupled oscillators. J. Theor. Biol. **16**, 15–42 (1967). https://doi.org/10.1016/0022-5193(67)90051-3
11. Kuramoto, Y.: Self-entrainment of a population of coupled non-linear oscillators. In: Araki, H. (ed.) International Symposium on Mathematical Problems in Theoretical Physics, pp. 420–422. Springer, Berlin (1975). https://doi.org/10.1007/BFb0013365
12. Czolczynski, K., Perlikowski, P., Stefanski, A., Kapitaniak, T.: Clustering of non-identical clocks. Prog. Theor. Phys. **125**, 473–90 (2011). https://doi.org/10.1143/PTP.125.473
13. Pantaleone, J.: Synchronization of metronomes. Am. J. Phys. **70**, 1–9 (2002). https://doi.org/10.1119/1.1501118
14. Ulrichs, H., Mann, A., Parlitz, U.: Synchronization and chaotic dynamics of coupled mechanical metronomes. Chaos **19**, 1–6 (2009). https://doi.org/10.1063/1.3266924
15. Czolczynski, K., Perlikowski, P., Stefanski, A., Kapitaniak, T.: Huygens' odd sympathy experiment revisited. Int. J. Bifurc. Chaos **21**, 2047–56 (2011). https://doi.org/10.1142/S0218127411029628
16. Czolczynski, K., Perlikowski, P., Stefanski, A., Kapitaniak, T.: Clustering and synchronization of n Huygens' clocks. Phys. A Stat. Mech. Appl. **388**, 5013–23 (2009). https://doi.org/10.1016/j.physa.2009.08.033
17. Czolczynski, K., Perlikowski, P., Stefanski, A., Kapitaniak, T.: Clustering of Huygens' clocks. Prog. Theor. Phys. **122**, 1027–33 (2009). https://doi.org/10.1143/PTP.122.1027
18. Najdecka, A., Kapitaniak, T., Wiercigroch, M.: Synchronous rotational motion of parametric pendulums. Int. J. Nonlinear Mech. **70**, 84–94 (2015). https://doi.org/10.1016/j.ijnonlinmec.2014.10.008
19. Strzalko, J., Grabski, J., Wojewoda, J., Wiercigroch, M., Kapitaniak, T.: Synchronous rotation of the set of double pendula: experimental observations. Chaos **22**, 1–7 (2012). https://doi.org/10.1063/1.4740460
20. Kapitaniak, M., Lazarek, M., Nielaczny, M., Czolczynski, K., Perlikowski, P., Kapitaniak, T.: Synchronization extends the life time of the desired behavior of globally coupled systems. Sci. Rep. **4**, 4391 (2014). https://doi.org/10.1038/srep04391
21. Kapitaniak, M., Czolczynski, K., Perlikowski, P., Stefanski, A., Kapitaniak, T.: Synchronous states of slowly rotating pendula. Phys. Rep. **541**, 1–44 (2014)
22. Strogatz, S.H., Abrams, D.M., McRobie, A., Eckhardt, B., Ott, E.: Crowd synchrony on the Millennium Bridge. Nature **438**, 43–4 (2005). https://doi.org/10.1038/43843a
23. Strogatz, S.H.: Exploring complex networks. Nature **410**, 268–76 (2001). https://doi.org/10.1038/35065725
24. Osipov, G.V., Kurths, J., Zhou, C.: Synchronization in Oscillatory Networks. Springer, Berlin (2007)
25. Boccaletti, S., Latora, V., Moreno, Y., Chavez, M., Hwang, D.U.: Complex networks: structure and dynamics. Phys. Rep. **424**, 175–308 (2006). https://doi.org/10.1016/j.physrep.2005.10.009
26. Dörfler, F., Bullo, F.: Synchronization in complex networks of phase oscillators: a survey. Automatica **50**, 1539–64 (2014). https://doi.org/10.1016/j.automatica.2014.04.012
27. Pikovsky, A., Rosenblum, M., Kurths, J.: Synchronization: A Universal Concept in Nonlinear Sciences. Cambridge University Press, Cambridge (2003). https://doi.org/10.1063/1.1554136
28. Kapitaniak, T.: Continuous control and synchronization in chaotic systems system. Chaos Solitons Fractals **6**, 237–44 (1995)
29. Blazejczyk-Okolewska, B., Brindley, J., Czolczynski, K., Kapitaniak, T.: Antiphase synchronization of chaos by non-continuous coupling: two impacting oscillators. Chaos Solitons Fractals **12**, 1823–6 (2001). https://doi.org/10.1016/S0960-0779(00)00145-4
30. Rosenblum, M.G., Pikovsky, A.S., Kurths, J.: Phase synchronization of chaotic oscillators. Phys. Rev. Lett. **76**, 1804–7 (1996)
31. Pecora, L.M., Carroll, T.L.: Synchronization in chaotic systems. Phys. Rev. Lett. **64**, 821–4 (1990). https://doi.org/10.1103/PhysRevLett.64.821
32. Boccaletti, S., Kurths, J., Osipov, G., Valladares, D.L., Zhou, C.S.: The synchronization of chaotic systems. Phys. Rep. **366**, 1–101 (2002). https://doi.org/10.1016/S0370-1573(02)00137-0
33. Kurths, J., Boccaletti, S., Grebogi, C., Lai, Y.C.: Introduction: control and synchronization in chaotic dynamical systems. Chaos **13**, 126–7 (2003). https://doi.org/10.1063/1.1554606

34. Pyragiene, T., Pyragas, K.: Anticipatory synchronization via low-dimensional filters. Phys. Lett. Sect. A Gen. At. Solid State Phys. **381**, 1893–8 (2017). https://doi.org/10.1016/j.physleta.2017.04.005
35. Liu, X., Wu, C.: Fault-tolerant synchronization for nonlinear switching systems with time-varying delay. Nonlinear Anal. Hybrid Syst. **23**, 91–110 (2017). https://doi.org/10.1016/j.nahs.2016.06.005
36. Dörfler, F., Chertkov, M., Bullo, F.: Synchronization in complex oscillator networks and smart grids. Proc. Natl. Acad. Sci. **110**, 2005–10 (2013). https://doi.org/10.1073/pnas.1212134110
37. Blaabjerg, F., Teodorescu, R., Liserre, M., Timbus, A.V.: Overview of control and grid synchronization for distributed power generation systems. IEEE Trans. Ind. Electron. **53**, 1398–409 (2006). https://doi.org/10.1109/TIE.2006.881997
38. Witthaut, D., Timme, M.: Braess's paradox in oscillator networks, desynchronization and power outage. New J. Phys. **14**, 083036 (2012). https://doi.org/10.1088/1367-2630/14/8/083036
39. Filatrella, G., Nielsen, A.H., Pedersen, N.F.: Analysis of a power grid using a Kuramoto-like model. Eur. Phys. J. B **61**, 485–91 (2008). https://doi.org/10.1140/epjb/e2008-00098-8
40. Rohden, M., Sorge, A., Timme, M., Witthaut, D.: Self-organized synchronization in decentralized power grids. Phys. Rev. Lett. **109**, 1–5 (2012). https://doi.org/10.1103/PhysRevLett.109.064101
41. Baldoni, R., Corsaro, A., Querzoni, L., Scipioni, S., Piergiovanni, S.T.: Coupling-based internal clock synchronization for large-scale dynamic distributed systems. IEEE Trans. Parallel Distrib. Syst. **21**, 607–19 (2010). https://doi.org/10.1109/TPDS.2009.111
42. Klein, D.J., Lee, P., Morgansen, K.A., Javidi, T.: Integration of communication and control using discrete time Kuramoto models for multivehicle coordination over broadcast networks. IEEE J. Sel. Areas Commun. **26**, 695–705 (2008). https://doi.org/10.1109/CDC.2007.4434294
43. Wang, Y., Nunez, F., Doyle III, F.J.: Increasing sync rate of pulse-coupled oscillators via phase response function design: theory and application to wireless networks. IEEE Trans. Control Syst. Technol. **21**, 1455–62 (2013). https://doi.org/10.1109/TCST.2012.2205254
44. Simeone, O., Spagnolini, U., Bar-Ness, Y., Strogatz, S.H.: Distributed synchronization in wireless networks. IEEE Signal Process. Mag. **25**, 81–97 (2008). https://doi.org/10.1109/MSP.2008.926661
45. Piqueira, J.R.C.: Using bifurcations in the determination of lock-in ranges for third-order phase-locked loops. Commun. Nonlinear Sci. Numer. Simul. **14**, 2328–35 (2009). https://doi.org/10.1016/j.cnsns.2008.06.012
46. Correa, D.P.F., Wulff, C., Piqueira, J.R.C.: Symmetric bifurcation analysis of synchronous states of time-delayed coupled phase-locked loop oscillators. Commun. Nonlinear Sci. Numer. Simul. **22**, 793–820 (2015). https://doi.org/10.1016/j.cnsns.2014.08.004
47. Piqueira, J.R.C., Oliveira, M.Q., Monteiro, L.H.A.: Synchronous state in a fully connected phase-locked loop network. Math. Probl. Eng. (2006). https://doi.org/10.1155/MPE/2006/52356
48. Giardina, I.: Collective behavior in animal groups: theoretical models and empirical studies. HFSP J. **2**, 205–19 (2008). https://doi.org/10.2976/1.2961038
49. Saber-Olfati, R., Fax, J.A., Murray, R.M.: Consensus and cooperation in networked multi-agent systems. Proc. IEEE **95**, 215–33 (2007). https://doi.org/10.1109/JPROC.2010.2049911
50. Bemporad, A., Heemels, M., Johansson, M.: Networked Control Systems. Springer, Berlin (1978)
51. Kuramoto, Y., Battogtokh, D.: Coexistence of coherence and incoherence in nonlocally coupled phase oscillators: a soluble case. Nonlinear Phenom. Complex Syst. **4**, 380–5 (2002)
52. Abrams, D.M., Mirollo, R.E., Strogatz, S.H., Wiley, D.A.: Solvable model for chimera states of coupled oscillators. Phys. Rev. Lett. **101**, 1–4 (2008). https://doi.org/10.1103/PhysRevLett.101.084103
53. Abrams, D.M., Strogatz, S.H.: Chimera states for coupled oscillators. Phys. Rev. Lett. **93**, 174102 (2004). https://doi.org/10.1103/PhysRevLett.93.174102
54. Panaggio, M.J., Abrams, D.M.: Chimera states: coexistence of coherence and incoherence in networks of coupled oscillators. Nonlinearity **28**, 67–87 (2015). https://doi.org/10.1088/0951-7715/28/3/R67
55. Tinsley, M.R., Nkomo, S., Showalter, K.: Chimera and phase-cluster states in populations of coupled chemical oscillators. Nat. Phys. **8**, 662–5 (2012). https://doi.org/10.1038/nphys2371
56. Hagerstrom, A.M., Murphy, T.E., Roy, R., Hövel, P., Omelchenko, I., Schöll, E.: Experimental observation of chimeras in coupled-map lattices. Nat. Phys. **8**, 658–61 (2012). https://doi.org/10.1038/nphys2372
57. Martens, E.A., Thutupalli, S., Fourrière, A., Hallatschek, O.: Chimera states in mechanical oscillator networks. Proc. Natl. Acad. Sci. **110**, 10563–7 (2013). https://doi.org/10.1073/pnas.1302880110
58. Kapitaniak, T., Kuzma, P., Wojewoda, J., Czolczynski, K., Maistrenko, Y.: Imperfect chimera states for coupled pendula. DINAME **2015**, 6 (2015). https://doi.org/10.1038/srep06379
59. Wojewoda, J., Czolczynski, K., Maistrenko, Y., Kapitaniak, T.: The smallest chimera state for coupled pendula. Sci. Rep. **6**, 34329 (2016). https://doi.org/10.1038/srep34329
60. Wolf, A., Swift, J.B., Swinney, H.L., Vastano, J.A.: Determining Lyapunov exponents from a time series. Physica D **16**, 285–317 (1985)

Publisher's Note Springer Nature remains neutral with regard to jurisdictional claims in published maps and institutional affiliations.